Computer Methods in Biomechanics and Biomedical Engineering

ISSN: 1025-5842 (Print) 1476-8259 (Online) Journal homepage: https://www.tandfonline.com/loi/gcmb20

Personalized hip joint kinetics during deep squatting in young, athletic adults

Jan Van Houcke, Pavel E. Galibarov, Gilles Van Acker, Sigrid Fauconnier, Ellen Allaert, Tom Van Hoof, Diogo F. Almeida, Gunther Steenackers, Christophe Pattyn & Emmanuel A. Audenaert

To cite this article: Jan Van Houcke, Pavel E. Galibarov, Gilles Van Acker, Sigrid Fauconnier, Ellen Allaert, Tom Van Hoof, Diogo F. Almeida, Gunther Steenackers, Christophe Pattyn & Emmanuel A. Audenaert (2019): Personalized hip joint kinetics during deep squatting in young, athletic adults, Computer Methods in Biomechanics and Biomedical Engineering, DOI: 10.1080/10255842.2019.1699539

To link to this article: https://doi.org/10.1080/10255842.2019.1699539

Published online: 06 Dec 2019.

COMPUTER METHODS IN BIOMECHANICS AND BIOMEDICAL ENGINEERING
https://doi.org/10.1080/10255842.2019.1699539

Personalized hip joint kinetics during deep squatting in young, athletic adults

Jan Van Houcke[a], Pavel E. Galibarov[b], Gilles Van Acker[a], Sigrid Fauconnier[a], Ellen Allaert[a], Tom Van Hoof[c], Diogo F. Almeida[a], Gunther Steenackers[d], Christophe Pattyn[a] and Emmanuel A. Audenaert[a,d]

[a]Department of Orthopaedic Surgery and Traumatology, University Hospital Ghent, Ghent, Belgium; [b]Anybody Technology A/S, Aalborg, Denmark; [c]Department of Anatomy and Embryology, Ghent University, Ghent, Belgium; [d]Department of Electromechanics, Op3Mech Research Group, University of Antwerp, Antwerpen, Belgium

ABSTRACT

The goal of this study was to report deep squat hip kinetics in young, athletic adults using a personalized numerical model solution based on inverse dynamics. Thirty-five healthy subjects underwent deep squat motion capture acquisitions and MRI scans of the lower extremities. Musculoskeletal models were personalized using each subject's lower limb anatomy. The average peak hip joint reaction force was 274 percent bodyweight. Average peak hip and knee flexion angles were 107° and 112° respectively. These new findings show that deep squatting kinetics in the younger population differ substantially from the previously reported in vivo data in older subjects.

ARTICLE HISTORY
Received 15 January 2019
Accepted 27 November 2019

KEYWORDS
Hip joint; loading; squat; motion capture; musculoskeletal model

Introduction

A deep squat requires high range of motion of the hip and knee joint (Bagwell et al. (2016); Shelburne and Pandy 2002; Smith et al. 2008). Repititive end range hip flexion has been shown to contribute to young adult hip pain in some mechanical hip disorders (Philippon et al. 2007; Lamontagne et al. 2009). Furthermore, it is hypothesized that premature conflicts between femur and acetabulum and high cartilage contact stresses can lead to early osteoarthritis of the hip joint (Mavcic et al. 2002; Ganz et al. 2008). Clearly some variations in hip morphology are pathological however in most cases the morphological abnormality is more discrete and difficult to identify (Reijman et al. 2005; Hosnijeh et al. 2017). The calculation of individual hip joint stresses using discrete or finite element analysis could potentially identify at-risk hip joints (Genda et al. 2001; Mavcic et al. 2002). However this computational simulation technique requires the input of accurate hip joint loading data during challenging hip joint motions such as the deep hip flexion squatting motion.

As a closed chain exercise, the squat has gained wide acceptance for core stabilization and strengthening the lower body muscles (Schoenfeld 2010). Previously, the lower limb joint kinematics have been described as well as the impact of variations in squatting technique (McLaughlin et al. 1977; Escamilla et al. 2001a; Swinton et al. 2012). Most of these studies have focused on the knee biomechanics with the aim of enhancing the strength performance and minimizing the injury risk (Wilk et al. 1996; Salem et al. 2003; Adouni and Shirazi-Adl 2009; Bersini et al. 2016). As such, the closed chain nature of the squat has been shown to reduce the anterior cruciate ligament strain thereby proving its rehabilitation superiority compared to the knee extension exercise (Yack et al. 1993; Signorile et al. 1994). Even though some of these studies also calculated knee joint reaction forces during deep squatting (Dahlkvist et al. 1982; Wilk et al. 1996; Escamilla et al. 2001b; Han et al. 2013), none report on the hip joint reaction force (HJRF) during deep squatting in young adults.

The golden standard in determining HJRF consists of in vivo measurements with the help of instrumented hip prostheses able to transmit data telemetrically (Rydell 1966; English and Kilvington 1979; Graichen and Bergmann 1991; Bergmann et al. 2001). Bergmann et al. have gathered the largest in vivo data sets currently available in literature and they report a mean peak HJRF of 147 percent of bodyweight (%BW) in 3 subjects (Bergmann et al. 2001) and 230%BW in 10 subjects (Bergmann et al. 2016)

CONTACT Jan Van Houcke jan.vanhoucke@ugent.be

during closed-chain squatting. Unfortunately, these subjects had to be eligible for a hip replacement and therefore their age is well over 50 years old. As a consequence, squatting depth was limited to approximately 47° of hip flexion and 75° of knee flexion. Clearly, flexion angles during deep squatting in young adults exceed these numbers with hip flexion angles of 95°-113° and knee flexion up to 153° (Hemmerich et al. 2006; Bagwell et al. 2016). As an alternative to the direct measurement of HJRF, which is ethically unfeasible in healthy subjects, new numerical models based on inverse dynamics have been developed that allow in silico calculation of HJRF (Damsgaard et al. 2006; Seth et al. 2011).

So far there have been no comprehensive reports on hip joint loading during deep squatting in young, athletic adults. The main goal of this study was therefore to report the HJRF during deep squatting in young, athletic adults using a subject specific modeling approach. Secondly, the associated hip range of motion, anterior pelvic tilt, knee flexion and hip joint moments were reported.

Methods

Subjects

Healthy subjects, aged 18 to 25 years old, were prospectively recruited in the local student community. Ethical clearance was obtained from the Ghent University Hospital's ethical board and all subjects signed an informed consent prior to data collection. Inclusion criteria were male gender, practicing more than 3 hours of sports weekly and body mass index below 25 kg/m2. Subjects were excluded in case there was any history of specific hip symptoms that could affect squatting kinematics. Furthermore, all subjects underwent a bilateral clinical hip examination in order to detect potential intra-articular hip pathology. Two subjects were not included because they reported pain during the FADIR test (Martin and Sekiya 2008; Reiman et al. 2015) or had a difference in knee to table distance between both hips of more than 5 cm during the FABER test (Philippon et al. 2007). A total number of 35 asymptomatic subjects was included. Demographic and anthropometric variables were documented in Table 1.

Data collection

First, subjects were trained to perform a smooth deep squat during at least 5 trials. They were instructed to position the feet shoulder width apart, to maintain heel contact throughout the squat and to extend their arms in front of them. A bench at approximately one third of the tibial crest height was placed behind the subject to guide them towards the deep squat during training (Lamontagne et al. 2009; Bagwell et al. 2016).

Three-dimensional kinetics were collected using a custom 8 camera OptiTrack motion capture system (Natural Point, Corvallis, Oregon, USA) synchronized with 2 force platforms (Kistler Instrument AG, type 9260AA, 30cmx50cm, Winterthur, Switzerland). The OptiTrack system has been shown to deliver

Table 1. Demographics, anthropometrics and kinetical results during full squat cycle from study group of 35 young, athletic subjects.

	Mean (95 CI)
Age (years)	21.9 (21.2–22.7)
Height (cm)	182 (180–184)
Weight (kg)	70.7 (68.0–73.4)
BMI (kg/m^2)	21.4 (20.8–22.0)
Sports (hours per week)	3.8 (3.1–4.5)
Neck-shaft angle (°)	129.6 (128.0–131.2)
Femoral version (°)	9.5 (7.0–11.9)
Duration squat (s)	4.2 (4.17–4.24)
Peak knee flexion (°)	112 (108.1–116.5)
Peak hip flexion (°)	107 (104.6–109.4)
Peak anterior pelvic tilt (°)	27 (24.2–30.2)
Peak hip abduction (°)	17 (15.1–19.6)
Peak hip internal rotation (°)	11 (9.0–13.6)
Peak hip joint reaction force (%BW)	274 (251.5–297.9)
Peak hip extension moment (Nm/kg)	0.56 (0.506–0.617)
Peak hip adduction moment (Nm/kg)	0.22 (0.184–0.248)
Peak hip internal rotation moment (Nm/kg)	0.12 (0.081–0.151)

95CI: 95% confidence interval between brackets. The neck shaft angle (Boese et al. 2016) was defined as the angle between the femoral neck axis (line connecting the centre of best fitting sphere of the femoral head and the centre of the femoral neck) and the anatomical femoral shaft axis (line connecting the centres of the best fitting circle of the proximal and distal diaphyseal femur). The femoral version (Victor et al. 2009; Casciaro and Craiem 2014) was defined as the angle between the femoral neck axis and the femoral transverse axis (line connecting the centres of the best fitting spheres of the medial and lateral femoral condyles).

comparable accuracy compared to high-end competitors with absolute errors below 1% (Thewlis et al. 2013).

The movements of the test subject during the experiment were tracked with passive, retroreflective markers (12 millimetre) applied to the subject's skin using double sided adhesive tape. In a standardized fashion, twenty-eight markers were placed on bony landmarks at the level of the pelvis, lower limb and seventh cervical vertebra by the same investigator. Three consecutive squat trials (standing – deep squat – standing) were captured with the subject standing with one foot on each force platform. The synchronized ground reaction force and motion capture data were fused into one comprehensive C3D file by means of the Biomechanical Toolkit (Barre and Armand 2014) in MATLAB (R2013a, MathWorks, Natick, Massachusetts, USA).

Next, the reflective markers were replaced with MRI compatible, hyperintense vitamin A beads taped to the skin at the same position. The subjects underwent a full lower limb MRI scan in a 3 Tesla Magnetom Trio-Tim System (Siemens, Erlangen, Germany). Dedicated T1 weighted sequences (MPRAGE, slice thickness 0.9 mm, pixel spacing 0.9 x 0.9 mm, repetition time 2200 milliseconds, echo time 2.38 milliseconds) were used. Mimics (Version 17.0, Materialise NV, Heverlee, Belgium) was used to process the individual MRI images and to perform semi-automatical segmentation of the bony contours of the pelvis, right thigh (femur) and right shank (tibia and fibula). Furthermore the position of the vitamin A beads was extracted from the MRI scan. These represent the reflective marker position in relation to the segmented bones.

Musculoskeletal modelling

The motion capture trajectories, force plate data, segmented bones (pelvis, thigh, shank) and position of the pelvic, thigh and shank markers were imported into a musculoskeletal multibody simulation environment. The Anybody Modeling System (version 7.0, AnyBody Technology, Aalborg, Denmark) with the AnyBody Managed Model Repository (version 2.0) and the TLEM 2.0 dataset were chosen (Carbone et al. 2015; Lund et al. 2017). This version includes a wrapping definition of the gluteus maximus muscle, which increases the lever arm of the muscle and avoids unphysiological bony surface penetration during deep hip flexion which is encountered in previous versions (Carbone et al. 2015; Varady et al. 2015)

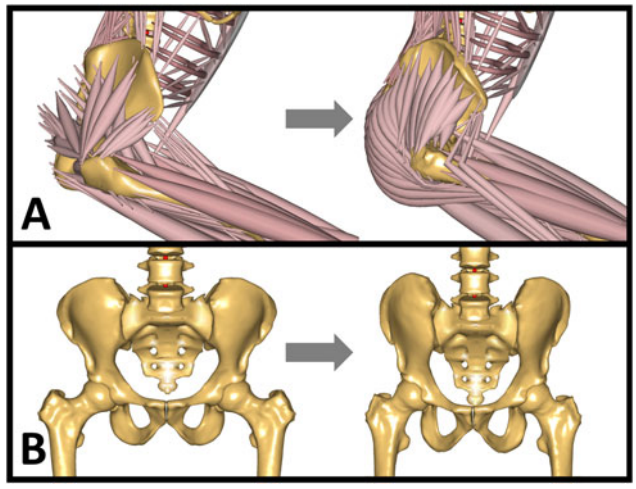

Figure 1. Musculoskeletal model features: (A) Left hand side shows the TLEM 1.0 musculoskeletal geometry. TLEM 2.0 on the right hand side includes improved detail in muscle geometry as well as physiological gluteal wrapping. (B) The generic TLEM 2.0 skeletal (and muscle) geometry on the left hand side was nonlinearly scaled to each subject, thereby accounting for changes in pelvic width, femoral version, etc.

(Figure 1). Standard topology of the AnyBody human model was used, which assumes the hip joint to be modeled as a ball-and-socket joint with 3 degrees of freedom and the knee as a hinge joint with one degree of freedom. Soft tissue strength parameters were adjusted using the standard length, mass, fat scaling law which takes BMI into account (Rasmussen et al. 2005). For the lower limb geometrical personalization, a novel automated workflow was combined with the motion capture processing model (AnyMoCap template model). First landmark correspondence between individual bone geometry and the AnyBody template bone was established using a previously developed nonrigid registration algorithm (Audenaert 2013). Next, automatic nonlinear scaling of the musculoskeletal geometry based on the individual bone geometries of pelvis, right thigh and right shank was performed. The left thigh and left shank were assumed to be symmetric and were similarly morphed using the mirrored right sided bones.

Additionally, the position of the pelvic, thigh and shank reflective markers relative to the bone was directly imported into the model using rigid transformation instead of estimating and optimizing marker position. Kinematic analysis was performed using an overdetermined kinematic solver to track the experimental markers in a least-squares sense (Andersen et al. 2009). Next, the resultant set of joint angle trajectories were used to drive the inverse dynamics and muscle recruitment optimization algorithms allowing calculation of the joint moments, muscle forces and

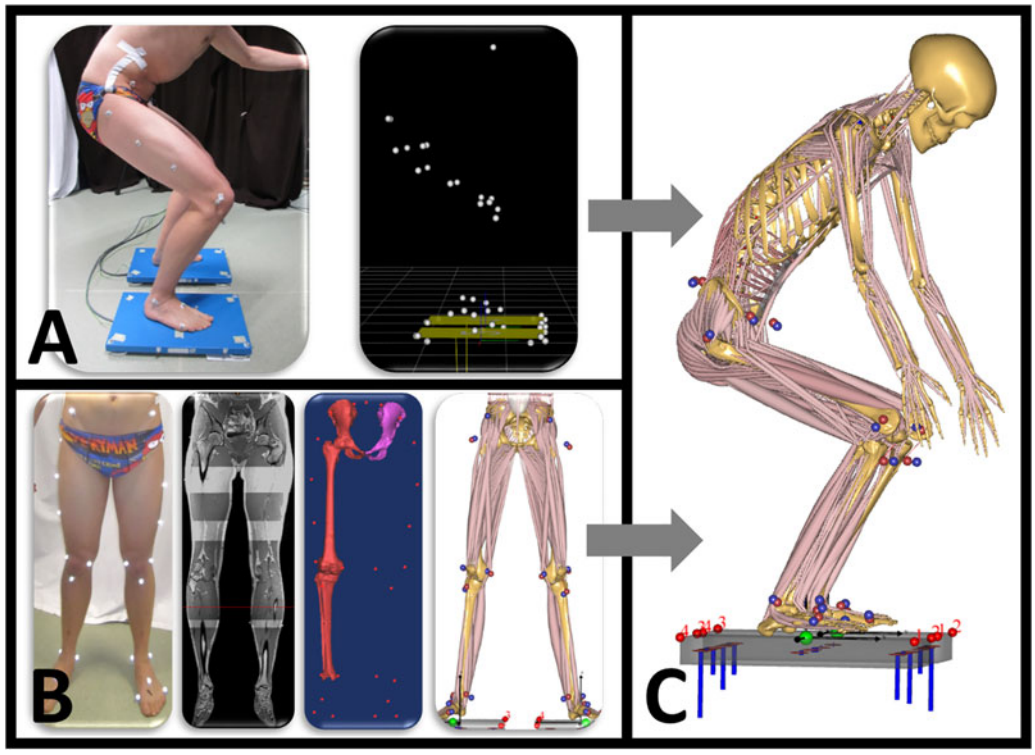

Figure 2. Overview of data input for the MoCap model. (A) Squat motion is performed standing on 2 forceplates. Motion capture data synchronized with ground reaction forces are exported as.c3d file. (B) A total of 28 reflective markers are placed on anatomical bony landmarks. An MRI scan of the full lower limb is performed. Segmentation of pelvis, thigh and shank with corresponding positions of marker landscape. (C) MoCap squat model.

joint reaction forces. Standard static optimization was used to minimize the third degree polynomial muscle recruitment criterion (Bean et al. 1988; Damsgaard et al. 2006). Subsequently the hip joint reaction forces were calculated from resultant inter-segment loading and muscle forces acting across the joint. The results presented are the joint constraint reactions. An overview of the musculoskeletal MoCap model is given in Figure 2.

Data processing

Local coordinate systems according to the ISB recommendations (Wu and Cavanagh 1995; Wu et al. 2002) were defined for the pelvis, thigh and shank. Subsequently, joint coordinate systems for the hip and knee joint were constructed in order to calculate three dimensional joint angles. The HJRF was projected in the pelvic local coordinate system. Squat trial recordings were trimmed from 0 to 100% of squat activity. The starting frame of the actual squat motion was manually identified by a continuous increase in knee and/or hip flexion. The end of the squat was identified by the return of both knee and hip flexion angles to the initial values at the time of standing upright. The deepest point of the squat, defined as peak knee flexion, was fixed at 50%. Since squatting speed is positively correlated with the joint reaction force generated (Hattin et al. 1989; Schoenfeld 2010), a partial least squares regression correction for the reaction force was introduced to account for squatting duration. All forces, moments and joints angles were measured at the right hip and knee. Internal hip joint moments were reported in the local femoral ISB coordinate system and were normalized by dividing the joint moment by body mass (Moisio et al. 2003).

Validation

The average knee bend trials from 3 subjects of the Orthoload database (Hip98; subjects HSR, KWR, PFL) were used for validation. The data available on these three subjects includes detailed kinematics, morphometrics (body weight and height) as well as in vivo measured HJRF results during the knee bend activity. This allowed a direct comparison of the in vivo measured HJRF of the Orthoload subjects to the average calculated HJRF of our study group. Furthermore, the retrieved kinematics and morphometrics of the knee bend trials could be used to run the presented musculoskeletal model in order to compare the estimated HJRF of each Orthoload knee

bend trial to the in vivo captured HJRF of the respective Orthoload knee bend trial. First, Orthoload joint angles were converted to ISB standards. Second, the Orthoload dataset was normalized from 0 to 100% of squat progression with 50% being the deepest point of the squat in order to facilitate comparison (see 2.4). The initial phase of the deep squat up to 75° of knee flexion and up to 47° hip flexion in our study group shows a similar HJRF pattern and then exceeds these values due to the deeper squatting (see Figure 3A). After all, peak knee and hip flexion is considerably lower in the older Orthoload subjects, which impedes a direct comparison of HJRF with the current deep squatting study population. For the purpose of validation, we therefore converted the motion capture driven model to a model driven by adjustable time and kinematical functions ('Driver model'). In doing so the Orthoload knee bend trials could be accurately simulated. A time dependent knee flexion function was defined in order to drive the squat motion. Additional drivers to control the body centre of mass, hip flexion, hip external rotation and hip abduction were included. The musculoskeletal definitions and muscle recruitment criterion of the Driver model were identical to the MoCap model (see 2.3). For each subject, the template model was scaled using external measurements (height, weight, thigh length and pelvis width) and driven to perform a similar squat motion. The calculated HJRF of the respective hip joint was then compared to the in vivo measured results. The goodness of fit of the HJRF curves was assessed using the root mean squared error (RMSE).

Results

Validation

The estimated HJRF during squat progression was slightly different compared to the in vivo values with an average RMSE of 16%BW. The estimated peak HJRF was on average 14%BW lower than in vivo measured (Figure 3 B-C-D).

Deep squat

Subjects were on average 21.9 years old, weighing 70.7 kg and measuring 182 cm. The femoral anatomy was within normal Caucasian ranges (Van Houcke et al. 2015), described by an average neck-shaft angle

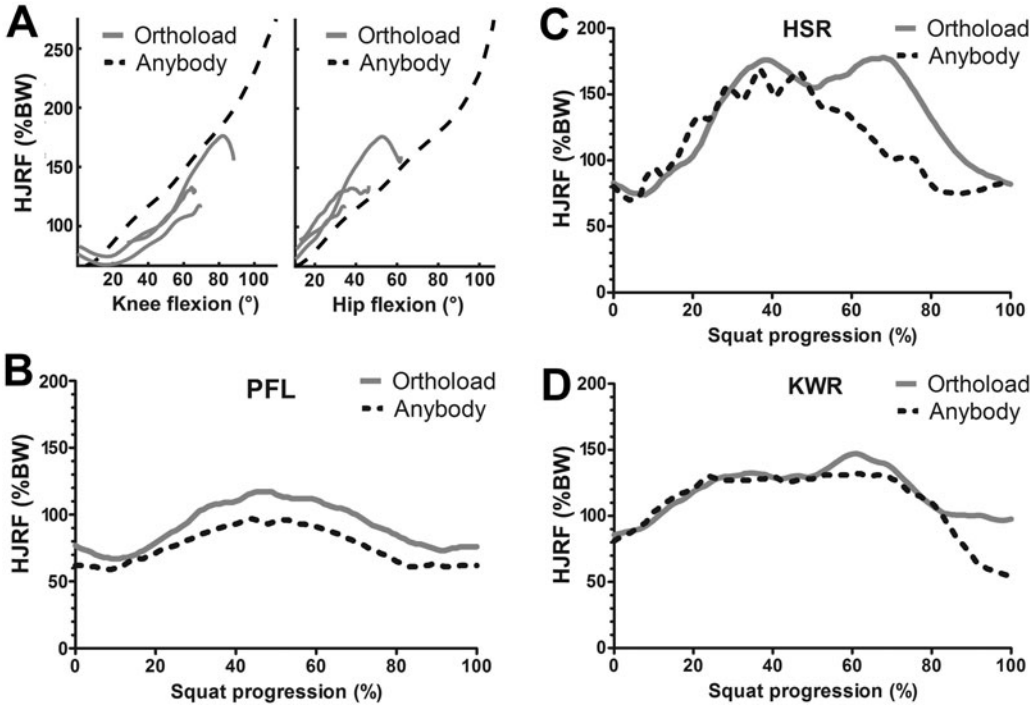

Figure 3. (A) Comparison of HJRF in function of knee and hip flexion respectively during the descending phase of the squat. The average HJRF of the current study group of 35 young, athletic subjects (performing a deep squat) is compared to the in vivo HJRF measurement of each of the three Orthoload subjects (PFL, HSR, KWR; performing shallow squats). (B,C,D) Musculuskeletal simulation of each squat experiment (respectively subject PFL, HSR and KWR) using the hip/knee kinematics and morphometrics to run the AnyBody Driver model. Comparison of the HJRF estimated with AnyBody Driver model versus the HJRF measured in vivo for each Orthoload subject separately. The solid grey line represents the in vivo measured HJRF (Orthoload), whereas the dotted black line represents the estimated HJRF (Anybody).

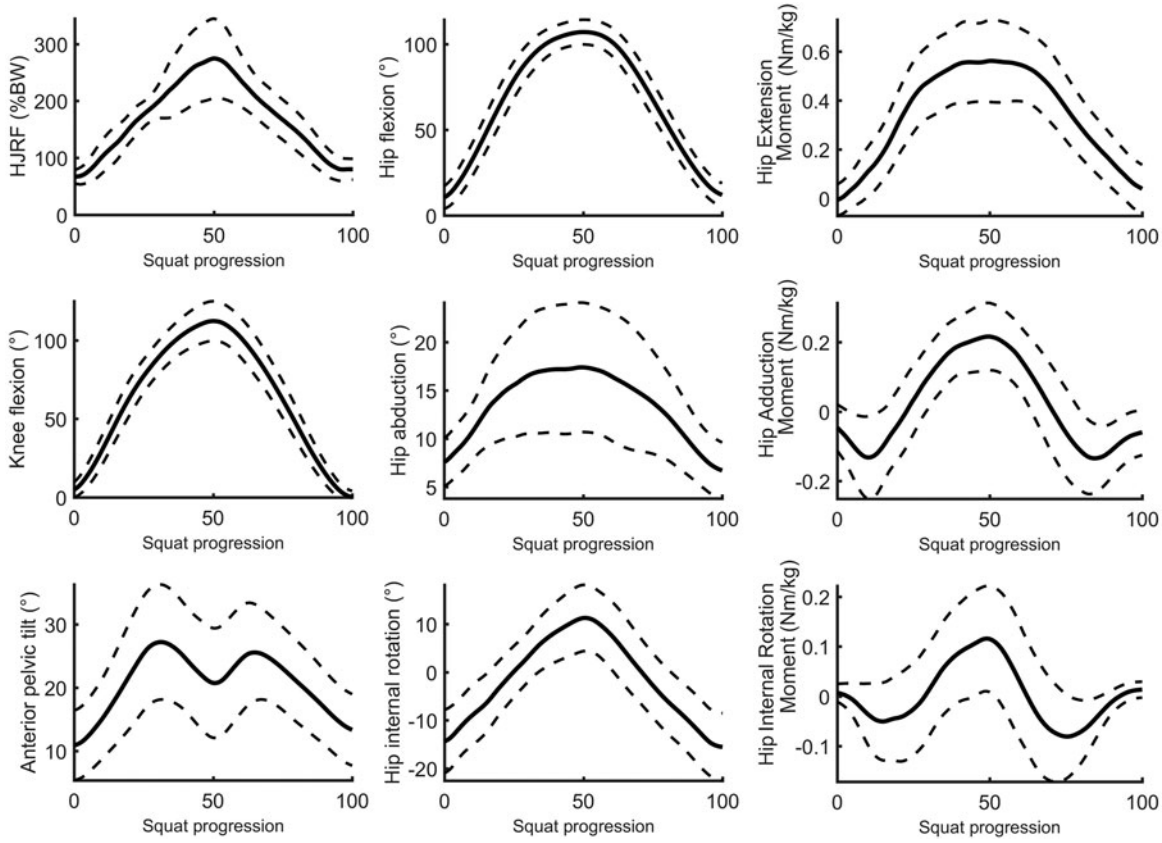

Figure 4. Overview of the calculated hip kinetics and knee flexion. The hip internal moments are at the deepest point of the squat a net extension, adduction and internal rotation moment. The solid line represents the group mean throughout squat cycle (0%: standing, 50%: deepest point of the squat, 0%: standing). The dashed line represents ±1 standard deviation.

of 129.6° and femoral anteversion of 9.5 degrees. The mean squat cycle duration was 4.2 seconds. Subjects squatted to a mean maximal value of 112° (108.1 – 116.5; 95% confidence interval) of knee flexion and 107° (104.6 – 109.4; 95% CI) of hip flexion. The resulting peak HJRF at the deepest point of the squat cycle was on average 274%BW (251.5 - 297.9; 95% CI). The HJRF on the pelvis was directed superior, medial and posterior throughout the activity. On average, subjects started the squat at 8° of hip abduction and reached a maximum of 17° (15.1 – 19.6; 95% CI) of abduction at the time of maximal squatting depth. The average external rotation of the femur was 14° at the start and amounted to 11° (9.0 – 13.6; 95% CI) of internal rotation at the time of maximal squatting depth. The anterior tilt of the pelvis increased from 11° to 27° during the first half of the descending phase of the squat. At the time of maximal squatting depth the anterior tilt decreased to 21°. The extension moment was the largest of the internal moments across the hip joint, peaking at 0.56 Nm/kg (0.506 – 0.617; 95% CI), with the adduction and internal rotation moment peaking at 0.22 Nm/kg (0.184 – 0.248, 95; CI) and 0.12 Nm/kg (0.081 – 0.151) respectively at the deepest point of the squat (Figure 4).

Discussion

This study estimated deep squat hip kinetics in young, athletic adults using a personalized numerical model solution based on inverse dynamics. The average peak HJRF was 274%BW at the time of maximal squatting depth. Average peak hip flexion, abduction and internal rotation were 107°, 17° and 11° respectively.

Direct comparison of HJRF calculation of our deep squat study group (MoCap model) with the in vivo Orthoload measurements in function of knee and hip flexion showed a similar pattern but reveals a potentially slightly different muscle coordination strategy during squatting. Indeed, our young subjects were trained to perform a deep squat with their arms extended in front of them. The Orthoload subjects performed a shallow squat with their arms crossed in front of the thorax. The simulation of each Orthoload subject's kinematics with the Driver model demonstrated a good agreement of HJRF results (model

calculation of peak HJRF during maximal squatting depth of 133%BW versus in vivo 147%BW). The first in vivo series of the Bergmann research group (2001) was used for the validation experiment since it contains the most detailed description of hip and knee kinematics to run the musculoskeletal model. Average peak hip and knee flexion in those cases was 47° and 75° respectively. Bergmann et al. (2016) published a second series of exclusively in vivo measured hip joint loading data. They reported an average HJRF of 230%BW in 10 patients which is 60% higher than the first series in 2001. They attributed the difference to an increased hip flexion and faster execution of the squat exercises. In our study, the average subject squatted to 112° of knee and 107° of hip flexion, thereby loading the hip joint at its peak with 274%BW. These values seem to match the expected increase in hip joint loading due to deeper squatting.

Previous studies based on musculoskeletal modelling have only reported HJRF values during shallow squatting. Weber et al. (2014) studied the influence of different surgical hip approaches when performing total hip arthroplasty on the resulting HJRF. They chose the squat motion to evaluate this effect and modelled a generic musculoskeletal model in AnyBody (using TLEM 1.0 muscle geometry) to perform a squat of 80° of knee and hip flexion over a timespan of 20 seconds. The loading of the reference hip joint, without any detached muscles, amounted to a peak value of 196% BW. In an exploratory study by Shelburne et al. (2010) on hip joint loading during squatting, a mean peak HJRF of 225%BW in a group of 10 subjects was found. Modelling was performed in OpenSim, but once again the sagittal motion of both hip and knee was limited to only 60°. It is likely that these computational studies have avoided pushing the musculoskeletal models to deep flexion, which results in hip joint loads of over 900%BW (Haberly and Pavol 2013; Varady et al. 2015). Figure 5 illustrates the drastically increased HJRF (mean peak of 419%BW) during deep squatting with implementation of the TLEM 1.0 muscle geometry. The TLEM 2.0 implementation with cylindrical wrapping of the gluteus maximus used in the current study provides a sufficient moment arm on the hip joint and unloads the hamstrings acting in their role of hip extensors. The gluteal muscles contribute to hip extension during the deeper stages of hip flexion and allow deep flexion with HJRF in a physiological range (Carbone et al. 2015; Varady et al. 2015).

Hip joint kinematics and internal moments corresponded well with the results of a recent study by

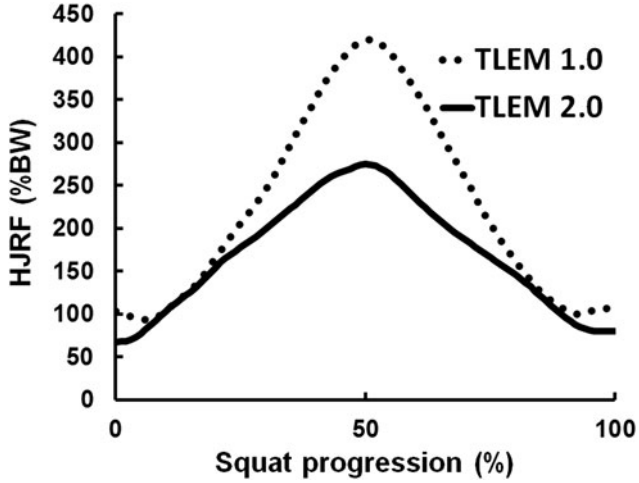

Figure 5. Comparison of the average HJRF in function of squat progression for the current study group of 35 subjects using TLEM 1.0 (solid black line; peak 419%BW) versus TLEM 2.0 (dotted black line; peak 274%BW).

Bagwell et al. (2016). They looked at deep squatting in a matched case-control study of 15 cam femoroacetabular impingement subjects versus 15 control subjects (average age 32 years old). In their control group, a peak hip flexion of 113° and peak anterior pelvic tilt at descending phase of 32° was reported. Our subjects had a mean hip flexion and anterior pelvic tilt that was slightly lower (respectively 107° and 27°). The reported hip joint moments matched our results with a mean extensor moment of 0.56 Nm/kg (vs 0.56 Nm/kg in our group), adductor moment of 0.09 Nm/kg (vs 0.22 Nm/kg) and internal rotation moment of 0.05 Nm/kg (vs 0.12 Nm/kg). The lower hip flexion and anterior pelvic tilt in the current study might be explained by the fact that our study group consisted of exclusively males whereas Bagwell's control group was mixed. It has been shown that hip and pelvic flexibility is significantly higher in young female adults (Mier and Shapiro 2013). A second explanation might be the high proportion of soccer players involved in our study group (13/35). Soccer players are known to exhibit lower ranges of hip joint motion (Manning and Hudson 2009).

The current model has been shown to adequately estimate the hip kinetics in young adults, however some limitations have to be considered. First, the validation is based on 3 elderly subjects that underwent total hip replacement, who likely have different squat techniques and muscle coordination strategies than the healthy individuals in this study. Additionally, the subject of the validation dataset did not go to deep squat which is the main investigation of this study. Nevertheless for the squatting range of motion documented in the Orthoload database a good agreement

was found between our simulated HJRF results and the original HJRF measurements. Second, skeletal motion was not measured directly and thus subject to both soft tissue artefacts as well as palpation errors (Della Croce et al. 2005; Fiorentino et al. 2017). In order to decrease the observer-dependent error caused by inevitable variation in palpating and determining the location of subcutaneous anatomical landmarks, the individual position of the reflective markers relative to the bone segment was directly determined from the MRI scan for the right thigh, right shank and the pelvis. For the left thigh and shank, marker positions relative to the bone were assumed to be equal to the right side. In order to minimize the impact of positional errors, care was taken to position the markers symmetrically during palpation. Furthermore, subjects were excluded if their BMI was higher than 25 kg/m2, thereby reducing the potential skin shift error caused by large soft tissue envelopes (Cappozzo et al. 1996). Moreover, our modelling pipeline included subject-specific pelvic, thigh and shank morphology, which eliminates the need for estimating the hip joint centre location based on skin marker motion alone. Inclusion of subject specific femoral geometry and hip joint centre location to the musculoskeletal model has been previously shown to drastically affect hip loading calculations (Scheys et al. 2008; Lenaerts et al. 2009). Third, both the Driver as well as the MoCap model only featured 1 degree of freedom (flexion-extension) at the knee joint. This simplification does not accurately reflect the human anatomy. Still, the 1 degree of freedom knee joint is widely used as standard configuration for simulation. The HJRF can be slightly overestimated as a consequence (Sandholm et al. 2011). However validation results showed a slight underestimation of the HJRF which might compensate for the overestimation effect of the uniplanar knee. Fourth, because of to the problem of muscle redundancy, there is always uncertainty about which muscles and how much they are involved during the motion. Selecting a suitable muscle recruitment criterion and including electromyographic data during motion capture could further reduce the potential error when calculating the resulting hip joint reaction force (Demers et al. 2014; Smith et al. 2019). Lastly the current study include only males, which limits the extrapolation of the results to females.

Conclusion

This study is the first to estimate deep squat hip kinetics in young, athletic adults using a personalized numerical model solution based on inverse dynamics. The average peak HJRF at the point of maximal depth squatting was found to be 274 percent bodyweight in young adults and as such substantially higher than the previously measured in vivo HJRF during shallow squatting of a limited number of total hip arthroplasty subjects. In the future these findings can allow comparison to hip loading of pathological hip morphologies. More importantly it can be used as input for deep squatting contact analysis studies of the hip in young adults.

Acknowledgements

The authors would like to thank Ashwin Schouten for his contribution to the musculoskeletal modelling.

Disclosure statement

Pavel Galibarov is an employee of AnyBody Technology. No financial benefits have been received or will be received from any commercial party related directly or indirectly to the subject of this article.

Funding

Jan Van Houcke was financially supported by PhD grant 11V2215N from the Research Foundation Flanders.

ORCID

Jan Van Houcke http://orcid.org/0000-0002-9738-7760

References

Adouni M, Shirazi-Adl A. 2009. Knee joint biomechanics in closed-kinetic-chain exercises. Comput Methods Biomech Biomed Eng. 12(6):661–670.

Andersen MS, Damsgaard M, Rasmussen J. 2009. Kinematic analysis of over-determinate biomechanical systems. Comput Methods Biomech Biomed Eng. 12(4): 371–384.

Audenaert EA. 2013. nonrigidICP, MATLAB central file exchange. [accessed 2016 November]. https://www.mathworks.com/matlabcentral/fileexchange/41396-nonrigidicp

Bagwell JJ, Snibbe J, Gerhardt M, Powers CM. 2016. Hip kinematics and kinetics in persons with and without cam femoroacetabular impingement during a deep squat task. Clin Biomech. 31:87–92.

Barre A, Armand S. 2014. Biomechanical ToolKit: Open-source framework to visualize and process biomechanical data. Comput Methods Programs Biomed. 114(1):80–87.

Bean JC, Chaffin DB, Schultz AB. 1988. Biomechanical model calculation of muscle contraction forces: a double linear programming method. J Biomech. 21(1):59–66.

Bergmann G, Bender A, Dymke J, Duda G, Damm P. 2016. Standardized Loads Acting in Hip Implants. PLoS One. 11(5):e0155612.

Bergmann G, Deuretzbacher G, Heller M, Graichen F, Rohlmann A, Strauss J, Duda GN. 2001. Hip contact forces and gait patterns from routine activities. J Biomech. 34(7):859–871.

Bersini S, Sansone V, Frigo CA. 2016. A dynamic multibody model of the physiological knee to predict internal loads during movement in gravitational field. Comput Methods Biomech Biomed Eng. 19(5):571–579.

Boese CK, Jostmeier J, Oppermann J, Dargel J, Chang DH, Eysel P, Lechler P. 2016. The neck shaft angle: CT reference values of 800 adult hips. Skeletal Radiol. 45(4): 455–463.

Cappozzo A, Catani F, Leardini A, Benedetti MG, Della Croce U. 1996. Position and orientation in space of bones during movement: experimental artefacts. Clin Biomech. 11(2):90–100.

Carbone V, Fluit R, Pellikaan P, van der Krogt MM, Janssen D, Damsgaard M, Vigneron L, Feilkas T, Koopman HF, Verdonschot N. 2015. TLEM 2.0 - a comprehensive musculoskeletal geometry dataset for subject-specific modeling of lower extremity. J Biomech. 48(5): 734–741.

Casciaro ME, Craiem D. 2014. Towards automatic measurement of anteversion and neck-shaft angles in human femurs using CT images. Comput Methods Biomech Biomed Eng. 17(2):128–136.

Dahlkvist NJ, Mayo P, Seedhom BB. 1982. Forces during squatting and rising from a deep squat. Eng Med. 11(2): 69–76.

Damsgaard M, Rasmussen J, Christensen ST, Surma E, de Zee M. 2006. Analysis of musculoskeletal systems in the AnyBody Modeling System. Simul Model Pract Theory. 14(8):1100–1111.

Della Croce U, Leardini A, Chiari L, Cappozzo A. 2005. Human movement analysis using stereophotogrammetry - part 4: assessment of anatomical landmark misplacement and its effects on joint kinematics. Gait Posture. 21(2):226–237.

Demers MS, Pal S, Delp SL. 2014. Changes in tibiofemoral forces due to variations in muscle activity during walking. J Orthop Res. 32(6):769–776.

English TA, Kilvington M. 1979. In vivo records of hip loads using a femoral implant with telemetric output (a preliminary report). J Biomed Eng. 1(2):111–115.

Escamilla RF, Fleisig GS, Lowry TM, Barrentine SW, Andrews JR. 2001. A three-dimensional biomechanical analysis of the squat during varying stance widths. Med Sci Sports Exercise. 33(6):984–998.

Escamilla RF, Fleisig GS, Zheng NQ, Lander JE, Barrentine SW, Andrews JR, Bergemann BW, Moorman CT. 2001. Effects of technique variations on knee biomechanics during the squat and leg press. Med Sci Sports Exercise. 33(9):1552–1566.

Fiorentino NM, Atkins PR, Kutschke MJ, Goebel JM, Foreman KB, Anderson AE. 2017. Soft tissue artifact causes significant errors in the calculation of joint angles and range of motion at the hip. Gait Posture. 55: 184–190.

Ganz R, Leunig M, Leunig-Ganz K, Harris WH. 2008. The etiology of osteoarthritis of the hip: an integrated mechanical concept. Clin Orthop Relat Res. 466(2):264–272.

Genda E, Iwasaki N, Li GA, MacWilliams BA, Barrance PJ, Chao E. 2001. Normal hip joint contact pressure distribution in single-leg standing - effect of gender and anatomic parameters. J Biomech. 34(7):895–905.

Graichen F, Bergmann G. 1991. 4-channel telemetry system for invivo measurement of hip-joint forces. J Biomed Eng. 13(5):370–375.

Haberly GJ, Pavol M. 2013. Hip loading during the squat exercise [master's thesis]. Corvallis (OR): Oregon State University.

Han S, Ge S, Liu H, Liu R. 2013. Alterations in three-dimensional knee kinematics and kinetics during neutral, squeeze and outward squat. J Hum Kinet. 39(1):59–66.

Hattin HC, Pierrynowski MR, Ball KA. 1989. Effect of load, cadence, and fatigue on tibio-femoral joint force during a half squat. Med Sci Sports Exercise. 21(5):613–618.

Hemmerich A, Brown H, Smith S, Marthandam SSK, Wyss UP. 2006. Hip, knee, and ankle kinematics of high range of motion activities of daily living. J Orthop Res. 24(4): 770–781.

Hosnijeh FS, Zuiderwijk ME, Versteeg M, Smeele HTW, Hofman A, Uitterlinden AG, Agricola R, Oei EHG, Waarsing JH, Bierma-Zeinstra SM. 2017. Cam deformity and acetabular dysplasia as risk factors for hip osteoarthritis. Arthritis Rheumatol. 69(1):86–93.

Lamontagne M, Kennedy MJ, Beaule PE. 2009. The effect of cam FAI on hip and pelvic motion during maximum squat. Clin Orthop Relat Res. 467(3):645–650.

Lenaerts G, Bartels W, Gelaude F, Mulier M, Spaepen A, Van der Perre G, Jonkers I. 2009. Subject-specific hip geometry and hip joint centre location affects calculated contact forces at the hip during gait. J Biomech. 42(9): 1246–1251.

Lund ME, Tørholm S, Galibarov PE, Jung M, Rasmussen KP, Gopalakrishnan A, Damsgaard M. 2017. The anybody managed model repository (AMMR) (version 2.0.0.). Zenodo. [accessed 2018 January]. https://zenodo.org/record/1251274#.XePYKJNKiCo

Manning C, Hudson Z. 2009. Comparison of hip joint range of motion in professional youth and senior team footballers with age-matched controls: an indication of early degenerative change? Phys Ther Sport. 10(1):25–29.

Martin RL, Sekiya JK. 2008. The interrater reliability of 4 clinical tests used to assess individuals with musculoskeletal hip pain. J Orthop Sports Phys Ther. 38(2):71–77.

Mavcic B, Pompe B, Antolic V, Daniel M, Iglic A, Kralj-Iglic V. 2002. Mathematical estimation of stress distribution in normal and dysplastic human hips. J Orthop Res. 20(5):1025–1030.

McLaughlin TM, Dillman CJ, Lardner TJ. 1977. A kinematic model of performance in the parallel squat by champion powerlifers. Med Sci Sports. 9(2):128–133.

Mier CM, Shapiro BS. 2013. Sex differences in pelvic and hip flexibility in men and women matched for sit-and-reach score. J Strength Cond Res. 27(4):1031–1035.

Moisio KC, Sumner DR, Shott S, Hurwitz DE. 2003. Normalization of joint moments during gait: a comparison of two techniques. J Biomech. 36(4):599–603.

Philippon MJ, Maxwell RB, Johnston TL, Schenker M, Briggs KK. 2007. Clinical presentation of femoroacetabular impingement. Knee Surg Sports Traumatol Arthr. 15(8):1041–1047.

Rasmussen J, Zee M, Damsgaard M, Christensen ST, Marek C, Siebertz K. 2005. A general method for scaling musculo-skeletal models. In 2005 International Symposium on Computer Simulation in Biomechanics and Modeling in Mechanobiology.

Reijman M, Hazes JMW, Pols HAP, Koes BW, Bierma-Zeinstra S. 2005. Acetabular dysplasia predicts incident osteoarthritis of the hip the Rotterdam study. Arthritis Rheum. 52(3):787–793.

Reiman MP, Goode AP, Cook CE, Holmich P, Thorborg K. 2015. Diagnostic accuracy of clinical tests for the diagnosis of hip femoroacetabular impingement/labral tear: a systematic review with meta-analysis. Br J Sports Med. 49(12):811.

Rydell NW. 1966. Forces acting on the femoral head-prosthesis. A study on strain gauge supplied prostheses in living persons. Acta Orthop Scand. 37(sup88):1–132.

Salem GJ, Salinas R, Harding FV. 2003. Bilateral kinematic and kinetic analysis of the squat exercise after anterior cruciate ligament reconstruction. Arch Phys Med Rehabil. 84(8):1211–1216.

Sandholm A, Schwartz C, Pronost N, de Zee M, Voigt M, Thalmann D. 2011. Evaluation of a geometry-based knee joint compared to a planar knee joint. Vis Comput. 27(2):161–171.

Scheys L, Van Campenhout A, Spaepen A, Suetens P, Jonkers I. 2008. Personalized MR-based musculoskeletal models compared to rescaled generic models in the presence of increased femoral anteversion: effect on hip moment arm lengths. Gait Posture. 28(3):358–365.

Schoenfeld BJ. 2010. Squatting kinematics and kinetics and their application to exercise performance. J Strength Cond Res. 24(12):3497–3506.

Seth A, Sherman M, Reinbolt JA, Delp SL. 2011. OpenSim: a musculoskeletal modeling and simulation framework for in silico investigations and exchange. Iutam Symposium on Human Body Dynamics, Waterloo, Canada. p. 212–232.

Shelburne KB, Decker MJ, Peterson D, Torry MR, Philippon MJ. 2010. Hip joint forces during squatting exercise predicted with subject-specific modeling. 56th Annual Meeting of the Orthopaedic Research Society, New Orleans, Lousiana.

Shelburne KB, Pandy MG. 2002. A dynamic model of the knee and lower limb for simulating rising movements. Comput Methods Biomech Biomed Eng. 5(2):149–159.

Signorile JF, Weber B, Roll B, Caruso JF, Lowensteyn I, Perry AC. 1994. An electromyographical comparison of the squat and knee extension exercises. J Strength Cond Res. 8(3):178–183.

Smith CR, Brandon SCE, Thelen DG. 2019. Can altered neuromuscular coordination restore soft tissue loading patterns in anterior cruciate ligament and menisci deficient knees during walking? J Biomech. 82:124–133.

Smith SM, Cockburn RA, Hemmerich A, Li RM, Wyss UP. 2008. Tibiofemoral joint contact forces and knee kinematics during squatting. Gait Posture. 27(3):376–386.

Swinton PA, Lloyd R, Keogh JWL, Agouris I, Stewart AD. 2012. A biomechanical comparison of the traditional squat, powerlifting squat, and box squat. J Strength Cond Res. 26(7):1805–1816.

Thewlis D, Bishop C, Daniell N, Paul G. 2013. Next-generation low-cost motion capture systems can provide comparable spatial accuracy to high-end systems. J Appl Biomech. 29(1):112–117.

Van Houcke J, Yau WP, Yan CH, Huysse W, Dechamps H, Lau WH, Wong CS, Pattyn C, Audenaert EA. 2015. Prevalence of radiographic parameters predisposing to femoroacetabular impingement in young asymptomatic Chinese and white subjects. J Bone Joint Surg-Am. 97(4): 310–317. Vol

Varady PA, Glitsch U, Augat P. 2015. Loads in the hip joint during physically demanding occupational tasks: A motion analysis study. J Biomech. 48(12):3227–3233.

Victor J, Van Doninck D, Labey L, Van Glabbeek F, Parizel P, Bellemans J. 2009. A common reference frame for describing rotation of the distal femur: a ct-based kinematic study using cadavers. J Bone Joint Surg-Br. 91-B(5):683–690. Vol

Weber T, Al-Munajjed AA, Verkerke GJ, Dendorfer S, Renkawitz T. 2014. Influence of minimally invasive total hip replacement on hip reaction forces and their orientations. J Orthop Res. 32(12):1680–1687.

Wilk KE, Escamilla RF, Fleisig GS, Barrentine SW, Andrews JR, Boyd ML. 1996. A comparison of tibiofemoral joint forces and electromyographic activit during open and closed kinetic chain exercises. Am J Sports Med. 24(4):518–527.

Wu G, Cavanagh PR. 1995. ISB recommendations for standardization in the reporting of kinematic data. J Biomech. 28(10):1257–1260.

Wu G, Siegler S, Allard P, Kirtley C, Leardini A, Rosenbaum D. 2002. ISB recommendation on definitions of joint coordinate system of various joints for the reporting of human joint motion - part I: ankle, hip, and spine. J Biomech. 35(4):543–548.

Yack HJ, Collins CE, Whieldon TJ. 1993. Comparison of closed and open kinetic chain exercise in the anterior cruciate ligament-deficient knee. Am J Sports Med. 21(1):49–54.